

SEISMIC IMAGING OF GAS HYDRATE-BEARING SEDIMENTS USING COUPLED SEISMIC AND ELECTROMAGNETIC WAVES

Fabio I. Zyserman^a, Patricia M. Gauzellino^b and Juan E. Santos^c

^aCONICET, Fac. de Cs. Astronómicas y Geofísicas, UNLP, Paseo del Bosque s/n, 1900, La Plata, Argentina, zyserman@fcaglp.unlp.edu.ar

^bFac. de Cs. Astronómicas y Geofísicas, UNLP, Paseo del Bosque s/n, 1900, La Plata, Argentina, gauze@fcaglp.unlp.edu.ar

^cCONICET, Fac. de Cs. Astronómicas y Geofísicas, UNLP, Paseo del Bosque s/n, 1900, La Plata, Argentina and Department of Mathematics, Purdue University, 150 N. University Street, West Lafayette, Indiana, 47907-2067, USA, santos@fcaglp.unlp.edu.ar

Keywords: Maxwell equations, Biot equations, Finite elements, Gas-hydrate.

Abstract. This work presents a 2D numerical model to obtain seismic images of gas hydrate bearing sediments in fluid-saturated poroelastic media. The differential model consists in Maxwell equations for the electromagnetic wave fields and Biot's equations of motion for the seismic wave fields, coupled with a zero-order term representing electrokinetic effects. The numerical model combines the solution of Maxwell's equation using a mixed finite element procedure using the edge-element of Nedelec with a standard Galerkin method to solve Biot's equations of motion. Biot's equations are discretized employing a nonconforming finite element to approximate the solid displacement and the vector part of the Raviart-Thomas-Nedelec space of zero order to compute the fluid displacements. The subsurface is modeled as a 2D fluid-saturated layered porous medium under transverse-magnetic (TM) modes. A numerical example illustrates the capabilities of the procedure to image gas hydrate bearing sediments in the subsurface.

1 INTRODUCTION

In order to increase the hydrocarbon production, the applied geophysics is always looking for new exploration tools. This fact stimulates the possibility of carrying out numerical simulations of interactions between conventional electromagnetic and seismic techniques. Electrostatic effects are acoustic signals that arise when electromagnetic sources are turned on in the surface. This electrostatic process takes place in the Electric Double Layer (EDL). In general, the surface of the solid matrix becomes negatively charged and in a reaction to that, ions of opposite charge appear in a thin boundary layer of the surrounding fluid. Close to the surface the ions are attached to the solid (Stern layer). As one moves away from the contact the ions can move, forming the diffuse layer because of balance between electrical and thermal forces. Then, the movements of ions in the EDL will induce movements of fluid (pressure gradients) when an electromagnetic field is applied. This makes it possible to record a seismic response in surface. Also, the reciprocal process of recording electromagnetic disturbances generated by seismic sources is possible.

This paper expounds a simulation case study showing the application of electrostatic effects to gas hydrates which are a combination of water and natural gas (methane). Under specific conditions where pressure is high and temperature is low, they combine to form a solid icelike substance, (Ikelle and Amundsen, 2005; Ecker et al., 2000; Guerin and Goldberg, 2005). Methane gas hydrates are considered important as a potential energy resource.

The theoretical frame used here is the one developed by Pride (1994) in the form given in, e.g. Haines and Pride (2006), but some issues regarding Biot's equations had to be addressed in order to use them to model deformation and propagation of waves both in permafrost and gas-hydrate environments. Several works such as Thompson and Gist (1993); Thompson (2005); Thompson et al. (2005); Hornbostel and Thompson (2007); Thompson et al. (2007) have proposed and analyzed electrostatics as a prospecting tool. In addition, different authors have proposed distinct numerical approximation procedures for both phenomena, among them Haartsen and Pride (1997); Han and Wang (2001); Pain et al. (2005); Haines and Pride (2006); Santos (2009) can be mentioned.

In this work, the coupled Maxwell and Biot's equations of motion are solved in an fluid-saturated poroviscoelastic media with absorbing boundary conditions for the case of compressional and vertically polarized seismic waves coupled with the transverse magnetic polarization, PSVTM mode. These equations are discretized by rectangular finite elements in 2D. The vector electric field and the scalar magnetic field are computed using the rotated Raviart-Thomas-Nedelec space of zero order, (Raviart and Thomas, 1977; Nedelec, 1980). Besides, the nonconforming spaces defined in Douglas, Jr. et al. (1999) are used to approximate each component of the displacement vector in the solid phase and the displacement in the fluid phase is approximated using the vector part of the Raviart-Thomas-Nedelec mixed finite element space of zero order. The iterative nonoverlapping domain decomposition procedure used here allows to solve problems with a large number of unknowns and is "naturally parallelizable", see (Zyserman and Santos, 2000; Gauzellino et al., 2009).

2 PRIDE'S THEORY OF THE COUPLING-FIELDS

The electrostatic equations are a combination of Maxwell equations for electromagnetic fields and Biot's equations for porous media. Assuming an $e^{+i\omega t}$ temporal dependence, the Pride's equations (Pride, 1994) for the electric and magnetic fields E and H , the displacement vector of the solid u^s and the relative fluid displacement vector u^f , can be stated in the space-

frequency domain as follows:

$$(\sigma + i\epsilon\omega)E - \nabla \times H + L(\omega)\eta\kappa^{-1} [i\omega u^f - L(\omega)E] = J_e^{ext}, \quad (1)$$

$$\nabla \times E + i\omega\mu H = J_m^{ext}, \quad (2)$$

$$-\omega^2\rho_b u^s - \omega^2\rho_f u^f - \nabla \cdot \tau(u) = F^{(s)}, \quad (3)$$

$$-\omega^2\rho_f u^s + \eta\kappa^{-1} [i\omega u^f - L(\omega)E] + \nabla p_f = F^{(f)}, \quad (4)$$

$$\tau_{lm}(u) = 2G \varepsilon_{lm}(u^s) + \delta_{lm} (\lambda_c \nabla \cdot u^s - \alpha K_{av} \xi), \quad (5)$$

$$p_f(u) = -\alpha K_{av} \nabla \cdot u^s - K_{av} \nabla \cdot u^f. \quad (6)$$

In the electromagnetic context, σ, ϵ and μ are the electrical conductivity, the electrical permittivity and the magnetic permeability respectively, being J_e^{ext}, J_m^{ext} external electromagnetic sources. In the poroviscoelastic equations, (3) and (4), ϕ is the porosity and $\rho_b = \phi\rho_f + (1-\phi)\rho_s$, where ρ_s and ρ_f denote the mass densities of the solid grains composing the solid matrix and the saturant fluid; while $F^{(s)}$ and $F^{(f)}$ are external seismic sources. The fluid pressure on the solid is $p_f(u)$ and the expressions, $L(\omega)$ and κ are the dynamic coupling coefficient and the dynamic permeability (Johnston et al., 1987; Pride, 1994), respectively. The fluid viscosity is denoted by η . The stress tensor is $\tau_{lm}(u)$ and $\varepsilon_{lm}(u^s)$ stands for the strain tensors.

In the constitutive relations (5) and (6), G is the shear modulus of the bulk material, K_c is the bulk modulus of the saturated material and $\lambda_c = K_c - \frac{2G}{3}$. The Biot coupling coefficient (Biot, 1956a,b, 1962) is αK_{av} , being K_{av} the fluid-storage coefficient and $\alpha = 1 - K_m/K_s$, where K_m is the dry solid matrix bulk modulus and K_s is the solid grains bulk modulus. The zone of permafrost and gas hydrates is represented by moduli for composite media, where different solid grains constitute the mineral matrix and a portion of the pore space is occupied by ice or gas hydrate, admitting to cement the mineral matrix.

2.1 Viscoelastic moduli

In order to consider the natural attenuation of the subsurface, the (real) elastic moduli G, K_s and K_m are replaced by complex frequency dependent viscoelastic moduli. The viscoelastic model presented in (Liu et al., 1976) is used through the following formula (K_s and K_m are dealt in the same way):

$$\widehat{G}(\omega) = \frac{G}{A(\omega) - iB(\omega)}. \quad (7)$$

Here the frequency dependent functions A and B , associated with a continuous spectrum of relaxation times, characterize the viscoelastic behavior and are given by

$$A(\omega) = 1 - \frac{1}{\pi\widehat{Q}} \ln \frac{1 + \omega^2 T_1^2}{1 + \omega^2 T_2^2}, \quad B(\omega) = \frac{2}{\pi\widehat{Q}} \tan^{-1} \frac{\omega(T_1 - T_2)}{1 + \omega^2 T_1 T_2}.$$

The model parameters \widehat{Q}, T_1 and T_2 are taken such that the quality factor $Q(\omega) = \frac{B(\omega)}{A(\omega)}$ is approximately equal to the constant \widehat{Q} in the range of frequencies where the equations are solved. Values of \widehat{Q} range from $\widehat{Q} = 10$ for highly dissipative materials to about $\widehat{Q} = 1000$ for almost elastic ones.

2.2 PSVTM modelling equations

The equations are solved in the range of seismic frequencies. Thus, the electroseismic coupling coefficient L , the permeability κ and the electric conductivity σ are considered to be real.

The expression used to compute the real part of L is given by [Pride and Garambois \(2002\)](#)

$$L_0 = -\frac{\phi \varepsilon_0 \kappa_f \zeta}{T \eta} \left(1 - 2 \frac{\tilde{d}}{\Lambda}\right), \quad (8)$$

where $\varepsilon_0 \kappa_f$ the fluid electric permittivity, Λ is a geometric factor representing a weighted volume to surface ratio, T is the tortuosity factor and \tilde{d} is the length of the EDL (Debye length). The potential $\zeta = (0.01 + 0.025 \log_{10} C)$ depends on the chemical properties of the fluid, being C the electrolyte molarity. Furthermore, the conduction currents in the low frequency range (1-500 Hz), are of about 4 orders of magnitude bigger than displacement currents, so the term $i\epsilon\omega E$ can be neglected ([Haines and Pride, 2006](#)).

Since the modeling is based on electroseismic effect, $F^{(s)} = F^{(f)} = 0$. Also, it is reasonable to assume that the generation of an electric current due to the induced pressure gradient (feedback) can be neglected. Remark that this assumption allows the generated electromagnetic field to be decoupled from the poroviscoelastic response.

Therefore, under the previous considerations and an infinite solenoid as electromagnetic source, ([Ward and Hohmann, 1987](#); [Templin, 1995](#)), the electromagnetic fields are $(E_x(x, z), E_z(x, z))$ and $H_y(x, z)$; while the solid and fluid displacements are $(u_x^s(x, z), u_z^s(x, z))$ and $(u_x^f(x, z), u_z^f(x, z))$. Consider a 2D-rectangular domain $\Omega = \Omega^A \cup \Omega^B$, where Ω^A and Ω^B are related to the air and subsurface parts of Ω , respectively. The boundary of Ω is denoted by Γ (Γ^A and Γ^B) and the letters t, b, r , and l indicate the top, bottom, right and left edges (or computational boundaries). Then, for the PSVTM mode the equations, (1)-(6) can be rewritten as:

$$\text{curl}E + i\omega\mu H_y = -J_m^{ext} \text{ in } \Omega, \quad (9)$$

$$\sigma E_y - \text{curl}H = 0 \text{ in } \Omega, \quad (10)$$

$$-\omega^2 \rho_b u^s - \omega^2 \rho_f u^f - \nabla \cdot \tau = 0 \text{ in } \Omega^B, \quad (11)$$

$$-\omega^2 \rho_f u^s - \omega^2 g_0 u^f + i\omega \frac{\eta}{k_0} u^f + \nabla p_f = \frac{\eta}{k_0} L_0 E \text{ in } \Omega^B, \quad (12)$$

with boundary conditions

$$\sqrt{\frac{\sigma}{2\mu\omega}}(1-i)E \cdot \chi + H_y = 0, \text{ on } \Gamma, \quad (13)$$

$$\tau \cdot \nu = 0, \quad p_f = 0 \text{ on } \Gamma^{t,B}, \quad (14)$$

$$-\mathcal{G}(u) = i\omega \mathcal{D}\mathcal{S}(u) \quad \text{on } \Gamma^{l,b,r,B}, \quad (15)$$

where $g_0 = 1.5 \frac{\rho_f T}{\phi}$ is the mass coupling coefficient, $\mathcal{G}(u) = (-\tau(u)\nu\nu, \tau(u)\nu\chi, p_f)^t$ and $\mathcal{S}(u) = (u^s \cdot \nu, u^s \cdot \chi, u^f \cdot \nu)$. In these expressions, ν is the unit outer normal on Γ and χ is a unit tangent on Γ oriented counterclockwise. The positive definite matrix \mathcal{D} in (15) depends on Biot's medium properties, ([Santos et al., 2004a](#)), $\mathcal{D} = \mathcal{R}^{\frac{1}{2}} \mathcal{S}^{\frac{1}{2}} \mathcal{R}^{\frac{1}{2}}$, where $\mathcal{S} = \mathcal{R}^{-\frac{1}{2}} \mathcal{M}^{-\frac{1}{2}} \mathcal{R}^{-\frac{1}{2}}$, and

$$\mathcal{R} = \begin{pmatrix} \rho_b & 0 & \rho_f \\ 0 & \rho_b - \rho_f^2/g_0 & 0 \\ \rho_f & 0 & g_0 \end{pmatrix}, \quad \mathcal{M} = \begin{pmatrix} \lambda_c + 2G & 0 & \alpha K_{av} \\ 0 & G & 0 \\ \alpha K_{av} & 0 & K_{av} \end{pmatrix}. \quad (16)$$

The electromagnetic source takes the form of a magnetic dipole of infinite length, $J_m^{ext} = -i\omega\mu SI(\omega)\delta(x-x_f)\delta(z-z_f)\tilde{y}$ centered in (x_f, z_f) , with $I(\omega)$ being the electric current and S the area of this current loop.

Finally, it is important to point out that assuming a conductivity distribution as, $\sigma(x, z) = \sigma_p(z) + \sigma_s(x, z)$, where $\sigma_p(z)$ is the background conductivity and $\sigma_s(x, z)$ is the conductivity anomaly; it can be distinguished between primary electromagnetic field and secondary electromagnetic field. The former can be computed analytically, while to calculate the latter a finite element procedure is employed. The total field $E = E_p + E_s$ is found, and set as a part of the source in Biot's equation (12).

3 NUMERICAL PROCEDURE

In a first step, the secondary electromagnetic field is obtained, and then the poroviscoelastic equations are solved. The iterative nonoverlapping domain decomposition method at differential level is applied to both Maxwell and Biot equations. For each frequency ω , the idea is to divide the problem in a collection of small ones whose individual solution can be easily computed. This technique is simple to implement it on parallel computers. See Santos (1998); Zyserman et al. (1999); Zyserman and Santos (2000); Gauzellino et al. (2001, 2009).

3.1 Maxwell's equations

Denote by Ω_j the rectangular elements of the finite element partition of the domain Ω , and assume the domain decomposition exactly coincides with the finite element partition. Let (\cdot, \cdot) be the inner product in an element, and $\langle \cdot, \cdot \rangle$ the inner product on the boundary of an element. Also, denote by Γ_{jk} the common boundary between the adjacent elements Ω_j and Ω_k , and by B_j^a the intersection of Γ_j with the computational domain.

To approximate the electromagnetic fields E^h and H^h , the spaces V^h and W^h are defined as:

$$\begin{aligned} V^h &= \{E^h \in H(\text{curl}, \Omega) : E^h|_{\Omega_j} \in P_{0,1} \times P_{1,0}\}, \\ W^h &= \{H^h \in L^2(\Omega) : H^h|_{\Omega_j} \in P_{0,0}\}, \\ V_j^h &= V^h|_{\Omega_j}, \quad W_j^h = W^h|_{\Omega_j}, \end{aligned}$$

where $P_{1,0}$ indicates a polynomial of degree less or equal 1 in x and less or equal 0 in z . Note that these spaces are rotated Raviart-Thomas spaces of zero order (they may be used to solve second order elliptic problems using mixed methods). The degrees of freedom related to each element are four to the electric field ubicated in the midpoints of the sides and one to the magnetic field ubicated at the center of rectangle.

For hybridized domain decomposition, it is also necessary to introduce the Lagrange multiplier space,

$$\Pi^h = \{\ell^h : \ell^h|_{\Gamma_{jk}} = \ell_{jk}^h \in [P_0(\Gamma_{jk})]^2 \equiv \Pi_{jk}^h\},$$

where $P_0(\Gamma_{jk})$ denotes the constant functions defined on the boundaries of the elements. These Lagrange multipliers are related to the magnetic field.

The numerical procedure is defined as follow: Find $(E_j^{h,n+1}, H_j^{h,n+1}, \ell_{jk}^{h,n+1}) \in V_j^h \times W_j^h \times \Pi_{jk}^h$

such that

$$\begin{aligned}
 & (\sigma E_j^{h,n+1}, \psi)_{\Omega_j} - (H_j^{h,n+1}, \text{curl} \psi)_{\Omega_j} + \sum_{\Gamma_{jk} \cap \Gamma = \phi} \langle \beta_{jk} E_j^{h,n+1} \cdot \chi_j, \psi \cdot \chi \rangle_{\Gamma_{jk}} \\
 & + \langle (1-i) \sqrt{\frac{\sigma}{2\omega\mu}} E_j^{h,n+1} \cdot \chi_j, \psi \cdot \chi_j \rangle_{B_j^a} = \\
 & - (\sigma_s E_p, \psi)_{\Omega_j} - \sum_{\Gamma_{jk} \cap \Gamma = \phi} \langle \beta_{jk} E_k^{h,n} \cdot \chi_k - H_k^{h,n}, \psi \cdot \chi \rangle_{\Gamma_{jk}}, \quad \psi \in V_j^h, \tag{17}
 \end{aligned}$$

$$(\text{curl} E_j^{h,n+1}, \varphi)_{\Omega_j} + (i\omega\mu H_j^{h,n+1}, \varphi)_{\Omega_j} = 0, \quad \varphi \in W_j^h, \tag{18}$$

$$\ell_{jk}^{h,n+1} = \ell_{jk}^{h,n} - \beta_{jk} (E_j^{h,n+1} \cdot \chi_j + E_k^{h,n} \cdot \chi_k) \quad \text{on } \Gamma_{jk}, \quad \Gamma_{jk} \cap \Gamma = \phi. \tag{19}$$

The coefficient β_{jk} is chosen as $\beta_{jk} = \frac{1}{2} (\sqrt{\frac{\sigma_j}{2\omega\mu}} + \sqrt{\frac{\sigma_k}{2\omega\mu}})$. The electric fields will be the source for the poroviscoelastic equations.

3.2 Biot's equations

The Biot's equations are solved analogously to previous problem. A nonconforming finite element space is used to approximate the solid displacements, while the vector part of the Raviart-Thomas-Nedelec space of zero order is used to approximate the fluid displacements. For details of the method the reader can look up (Santos et al., 2004a,b, 2005). Specifically, determine

$$R = [-1, 1]^2, \quad \mathcal{NC}(R) = \text{Span}\{1, x, z, \alpha(x) - \alpha(z)\}, \quad \alpha(x) = x^2 - \frac{5}{3}x^4, \tag{20}$$

and $\varphi^L(x) = -1 + x$, $\varphi^R(x) = x$, $\varphi^B(z) = -1 + z$, $\varphi^T(z) = z$, set

$$\mathcal{RTN}(R) = \text{Span}\{(\varphi^L(x), 0), (\varphi^R(x), 0), (0, \varphi^B(z)), (0, \varphi^T(z))\}. \tag{21}$$

The degrees of freedom associated with each element are four for each solid displacement component and two for each fluid displacement component located at the midpoint of each edge of R .

The method of hybridization implemented requires the definition of a set of Lagrange multipliers which are associated to generalized forces on the interelement boundaries. Setting $v = (v^s, v^f) \in \mathcal{NC}_j^h \times \mathcal{RTN}_j^h$ and $\Lambda^h = \{\lambda^h : \lambda^h|_{\Gamma_{jk}} = \lambda_{jk}^h \in [P_0(\Gamma_{jk})]^2 \equiv \Lambda_{jk}^h\}$, where

$P_0(\Gamma_{jk})$ denotes the constant functions defined on Γ_{jk} . The algorithm is expressed as follow:

$$\begin{aligned}
 & -\omega^2 \left(\rho_b u_j^{s,h,n+1} + \rho_f u_j^{f,h,n+1}, v^s \right)_{\Omega_j^B} - \omega^2 \left(\rho_f u_j^{s,h,n+1} + g_0 u_j^{s,h,n+1}, v^f \right)_{\Omega_j^B} \\
 & + i\omega \left(g_0 u_j^{f,h,n+1}, v^f \right)_{\Omega_j^B} + \sum_{lm} \left(\tau_{lm}(v_j^{h,n+1}), \varepsilon_{lm}(v^s) \right)_{\Omega_j^B} \\
 & - \left(p_f(u_j^{h,n+1}), \nabla \cdot v^f \right)_{\Omega_j^B} + \left\langle \mathcal{S}(u_j^{s,h,n+1}), \mathcal{S}(v) \right\rangle_{\Gamma_j \cap \Gamma^{l,b,r,B}} \\
 & + \sum_{\Gamma_{jk} \cap \Gamma^B = \phi} \left\langle i\omega \beta_{jk} \mathcal{S}(u_j^{h,n+1}), \mathcal{S}(v) \right\rangle_{\Gamma_{jk}} = \left(\frac{\eta L_0}{k_0} (E_p + E_s), v^f \right)_{\Omega_j^B} \\
 & - \sum_{\Gamma_{jk} \cap \Gamma^B = \phi} \left\langle i\omega \beta_{jk} \mathcal{S}(u_k^{h,n}), \mathcal{S}(v) \right\rangle_{\Gamma_{jk}} + \sum_{\Gamma_{jk} \cap \Gamma^B = \phi} \left\langle \lambda_{kj}^{h,n}, \mathcal{S}(v) \right\rangle_{\Gamma_{jk}} \tag{22}
 \end{aligned}$$

$$\lambda_{jk}^{h,n+1} = \lambda_{kj}^{h,n} - i\omega \beta_{jk} \left[\mathcal{S}(u_j^{h,n+1}) + \mathcal{S}(u_k^{h,n}) \right] (\gamma_{jk}). \tag{23}$$

The parameter β_{jk} is a positive definite matrix, and is chosen as the average $\frac{1}{2}(\mathcal{D}_j + \mathcal{D}_k)$, where \mathcal{D} is the matrix appearing in the absorbing boundary conditions. The source is given by the total electric field, $(E_p + E_s)$, and the electroseismic coupling factor, L_0 .

4 RESULTS

The geological model is shown in Figure 1 and Table 1. The information of the physical parameters was obtained from Rubino et al. (2008) and Petrenko and Whitworth (1999). The electroseismic properties of the different layers are calculated by using composite and poro-viscoelastic models, that take into account the total gas hydrate saturation and the cementation coefficient.

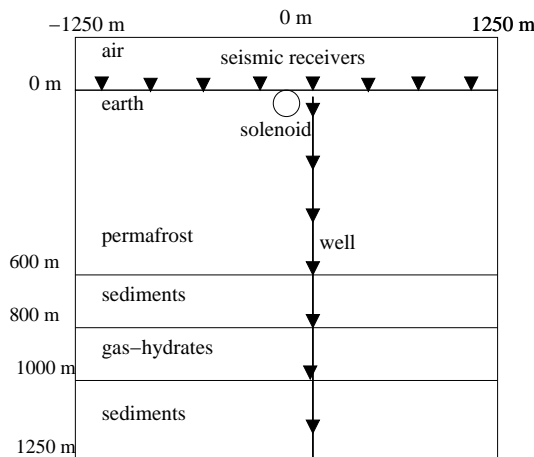


Figure 1: Layered subsurface with gas hydrate.

In this particular example, the gas hydrate saturation is only 10 % and without matrix cementation. The values of the electrical conductivity are $\sigma_{perm}=3.8 \cdot 10^{-3}$ S/m, $\sigma_{sedim}=0.3$ S/m and $\sigma_{gashy}=0.11$ S/m. Inside of the region with gas hydrates the electroseismic coupling coefficient

Medium	V_P [m/s]	V_S [m/s]	ϕ	κ [m ²]	K_{av} [Gpa]	K_c [Gpa]	α	g_0 [Kg/m ³]
Permafrost	4200	2300	0.11	$6.56 \cdot 10^{-12}$	48.9	22.5	0.15	$11.4 \cdot 10^9$
Sediment	2240	880	0.30	$1 \cdot 10^{-8}$	6.78	8.66	0.92	$1.7 \cdot 10^9$
Gas hydrate	3200	1620	0.30	$7.71 \cdot 10^{-9}$	7.55	14.53	0.70	$5.7 \cdot 10^9$

Table 1: Seismic properties of the layered subsurface.

was computed to be $L_0=2.45 \cdot 10^{-9}$ V/Pa and $2.75 \cdot 10^{-9}$ V/Pa for the sediments.

The bulk densities of each layer are as follows: $\rho_{b,perm}=2135$ Kg/m³, $\rho_{b,sedim}=2650$ Kg/m³ and $\rho_{b,gashy}=2150$ Kg/m³. The fluid is water whose density is $\rho_f=1030$ Kg/m³ y viscosity $\eta=0.018$ Poise.

In order to characterize viscoelasticity, the quality factor, Q , was chosen to be $\hat{Q} = 100$ for whole layers.

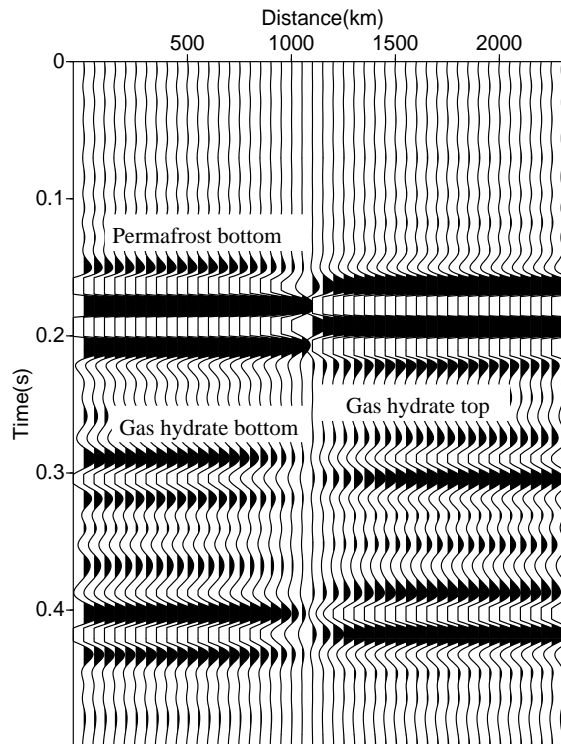


Figure 2: Example of 48 seismic traces at surface.

The computational domain has $2.500 \text{ km} \times 1.250 \text{ km}$ and comprises 3068×1534 elements. Seismic receivers are separated by a distance of 50 m and are spread along the surface. Observe that the Maxwell equations represent a diffusion process and the electroosmotic effect is due to the Biot's slow wave (diffusion type wave), therefore, the right way to simulate these phenomena is taken account at least two or four points per diffusion length, see (Haines and Pride, 2006). The CPU time running with 25 processors was 17 hours. The time dependence of the current in the electromagnetic source is given by a Ricker wavelet with a central frequency equal to 30 Hz. The equations (17), (18), (19), (22) and (23) are solved for 100 equally spaced samples of

frequency. Once all the results in the space-frequency domain are computed, they are inverse Fourier transformed to get the space-time responses.

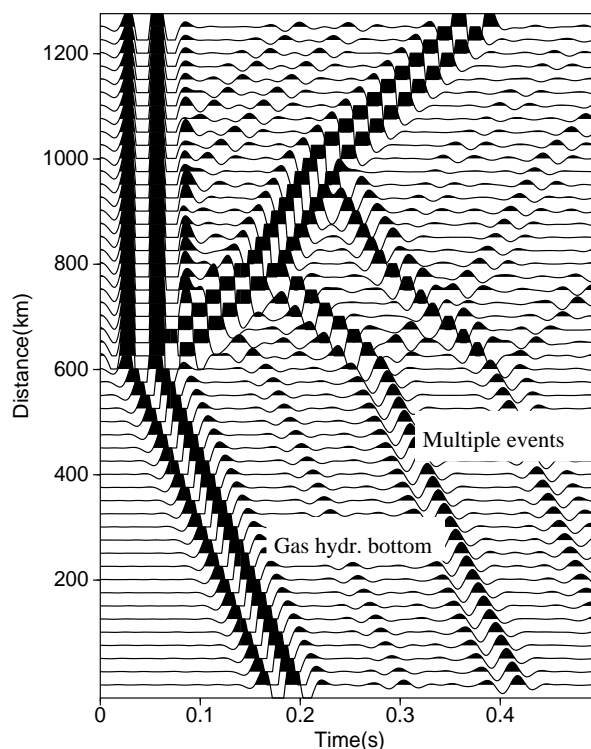


Figure 3: Example of 51 seismic traces in a well.

Figure 2 shows the seismic signals detected by accelerometers that are sensitive to the vertical particle-acceleration component and are located on the surface. Along the layer boundaries, the seismic sources are activated simultaneously to produce seismic waves that propagate in both directions of the time axis. The different arrival times indicate the depth of the horizons below the surface; in this case, they correspond to permafrost bottom at 0.142 s, gas hydrate top at 0.232 s and gas hydrate bottom at 0.295 s. The strong arrivals at 0.4 s are related to multiple reflections. Of course, this is based on the observations of vertical acceleration component in a well ubicated at 50 m from the electromagnetic source. Figure 3 shows the seismic signals in the well and it is possible to perform reliable correlations among time arrivals.

Snapshot of pressure field at $t=0.04$ s is presented in Figure 4. Notice that the significant amplitudes of the pressure field inform where the layer interfaces lie. So, wavefronts generated by these interfaces start to travel upward and downward.

5 CONCLUSIONS

Electroseismic theory, rock-physics models and numerical simulation of wave propagation have been used to study seismic images of gas hydrate bearing sediments. The procedures presented in this work can be implemented to distinguish seismic responses generated by electromagnetic fields for any subsurface and assist to development of new hydrocarbon exploration

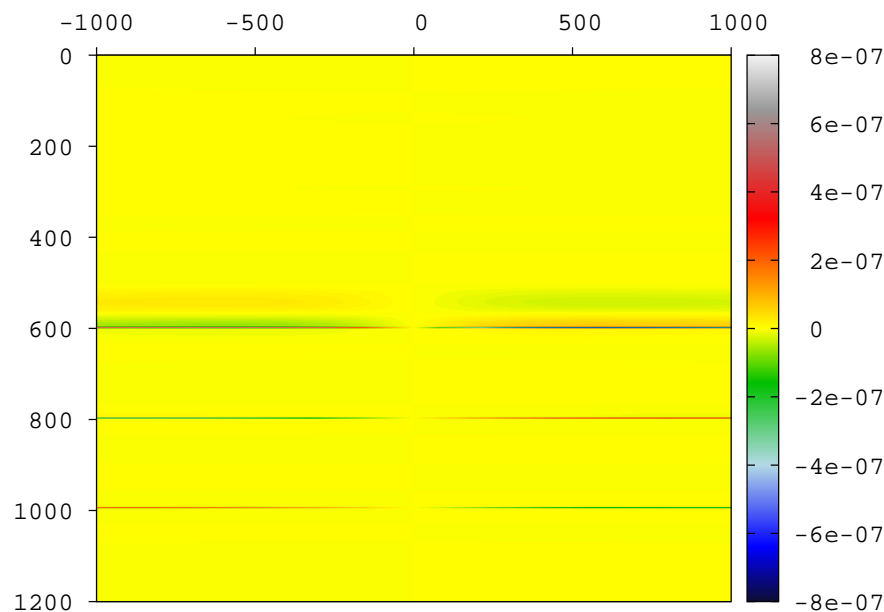


Figure 4: Snapshot of pressure field at $t=0.04$ s.

tools. It has been achieved, through numerical models, a seismic characterization of the different layers, including the gas hydrates. The strong events are those associated with multiple reflections, therefore it will be necessary to apply signal processing in order to obtain a clearer image of the interfaces.

6 ACKNOWLEDGEMENTS

This research was partially supported by CONICET, through grant PIP 112-200801-00952. We thank RCAC, Purdue University, since the parallel codes were run on the Steele cluster.

REFERENCES

- Biot M. Mechanics of deformation and acoustic propagation in porous media. *J. Appl. Phys.*, 33:1482–1498, 1962.
- Biot M.A. Theory of propagation of elastic waves in a fluid-saturated porous solid. I. Low frequency range. *Journal of the Acoustical Society of America*, 28:168–171, 1956a.
- Biot M.A. Theory of propagation of elastic waves in a fluid-saturated porous solid. II. High frequency range. *Journal of the Acoustical Society of America*, 28:179–191, 1956b.
- Douglas, Jr. J., Santos J.E., Sheen D., and X Y. Nonconforming Galerkin methods based on quadrilateral elements for second order elliptic problems. *RAIRO Mathematical Modelling and Numerical Analysis (M2AN)*, 33:747–770, 1999.
- Ecker C., Dvorkin J., and Nur A.M. Estimating the amount of gas hydrate and free gas from marine sediments. *Geophysics*, 65(2):565–573, 2000.
- Gauzellino P.M., Santos J.E., and Sheen D. Frequency domain wave propagation modelling in exploration seismology. *Journal of Computational Acoustics*, 9:941–955, 2001.
- Gauzellino P.M., Zyserman F.I., and Santos J.E. Nonconforming finite element methods for the three-dimensional helmholtz equation: Iterative domain decomposition or global solution ? *Journal of Computational Acoustics*, 17(2):159–173, 2009.

- Guerin G. and Goldberg D. Modeling of acoustic wave dissipation in gas hydrate-bearing sediments. *Geochemistry, Geophysics, Geosystems*, 6(7):1–16, 2005.
- Haartsen M.W. and Pride S.R. Electrostatic wave properties. *Journal Geophysical Research*, 102:24745–24756, 1997.
- Haines S.H. and Pride S.R. Seismoelectric numerical modeling on a grid. *Geophysics*, 71(6):57–65, 2006.
- Han Q. and Wang Z. Time-domain simulation of sh-wave-induced electromagnetic field in heterogeneous porous media: A fast finite element algorithm. *Geophysics*, 66(2):448–461, 2001.
- Hornbostel S. and Thompson A.H. Waveform design for electrostatic exploration. *Geophysics*, 72(2):Q1–Q10, 2007.
- Ikelle L. and Amundsen L. *Introduction to petroleum seismology*, volume No 12. Society of Exploration Geophysicists, USA, 2005.
- Johnston D.L., Koplik J., and Dashen R. Theory of dynamic permeability and tortuosity in fluid-saturated porous media. *J. Fluid Mechanics*, 176:379, 1987.
- Liu H.P., Anderson D.L., and Kanamori H. Velocity dispersion due to anelasticity; implications for seismology and mantle composition. *Geophys. J. R. Astr. Soc.*, 147:41–58, 1976.
- Nedelec J.C. Mixed finite elements in r^3 . *Numer. Math.*, 35:315, 1980.
- Pain C.C., Saunders J.H., Wortington M.H., Singer J.M., Stuart-Bruges W., Mason G., and Goddard A. A mixed finite element method for solving the poroelastic biot equations with electrokinetic coupling. *Geophys. J. Int.*, 160:592–608, 2005.
- Petrenko V.F. and Whitworth R.W. *Physics of Ice*. Oxford University Press, USA, 1999.
- Pride S. and Garambois S. The role of biot slow waves in electrostatic wave phenomena. *jasa*, 111(2):697–706, 2002.
- Pride S.R. Governing equations for the coupled electromagnetics and acoustics of porous media. *Physical Review B*, 50:15678–15696, 1994.
- Raviart P. and Thomas J. *A mixed finite element method for second order elliptic problems. Lecture notes in Mathematics.*, volume 606. Springer-Verlag, Berlin, New York, 1977.
- Rubino J.G., Ravazzoli C.L., and Santos J.E. Biot-type scattering effects in gas hydrate-bearing sediments. *Journal Geophysical Research*, 113:B06102, 2008.
- Santos J.E. Global and domain-decomposed mixed methods for the solution of Maxwell's equation with application to magnetotellurics. *Numerical Methods for Partial Differential Equations*, 14:263–280, 1998.
- Santos J.E. Finite element approximation of coupled seismic and electromagnetic waves in fluid-saturated poroviscoelastic media. *Aceptado para publicar en Numerical Methods for Partial Differential Equations*, 2009.
- Santos J.E., Ravazzoli C.L., and Carcione J.M. A model for wave propagation in a composite solid matrix saturated by a single-phase fluid. *Journal of the Acoustical Society of America*, 115(6):2749–2760, 2004a.
- Santos J.E., Ravazzoli C.L., Gauzellino P.M., and Carcione J.M. Numerical simulation of ultrasonic waves in reservoir rocks with patchy saturation and fractal petrophysical properties. *Computational Geosciences*, 9:1–27, 2005.
- Santos J.E., Ravazzoli C.L., Gauzellino P.M., Carcione J.M., and Cavallini F. Simulation of waves in poro-viscoelastic rocks saturated by immiscible fluids. numerical evidence of a second slow wave. *Journal of Computational Acoustics*, 12(1):1–21, 2004b.
- Templin J.D. Exact solution to the field equations in the case of an ideal, infinite solenoid. *Am. J. Phys.*, 63(10):916–920, 1995.

- Thompson A.H. Electromagnetic-to-seismic conversion: Successful developments suggest viable applications in exploration and production. In *75th SEG Annual Meeting Expanded Abstracts*. SEG, Houston, 2005.
- Thompson A.H. and Gist G. Geophysical applications of electrokinetic conversion. *The leading edge*, 12:1169–1173, 1993.
- Thompson A.H., Hornbostel S., Burns J., Murray T., Raschke R., Wride J., McCammon P., Sumner J., Haake G., Bixby M., Ross W., White B.S., Zhou M., and Peczak P. Field tests of electroseismic hydrocarbon detection. *Geophysics*, 72(1):N1–N9, 2007.
- Thompson A.H., Hornbostel S., Burns J., Murray T., Raschke R., Wride J., McCammon P., Sumner J., Haake G., M. Bixby W.R., White B., Zhou M., and Peczak P. Field tests of electroseismic hydrocarbon detection. In *75th SEG Annual Meeting Expanded Abstracts*, pages 565–568. SEG, Houston, 2005.
- Ward S. and Hohmann G.W. Electromagnetic theory for geophysical applications. In M.N. Nabighian, editor, *Electromagnetic Methods in Applied Geophysics*, volume 1 of *SEG Investigations in Geophysics 3*. SEG, 1987.
- Zyserman F.I., Guarracino L., and Santos J.E. A hybridized mixed finite element domain decomposed method for two-dimensional magnetotelluric modelling. *Earth, Planets and Space*, 51:297–306, 1999.
- Zyserman F.I. and Santos J.E. Parallel finite element algorithm for three-dimensional magnetotelluric modelling. *Journal of Applied Geophysics*, 44:337–351, 2000.